*Desalination and Water Treatment*
www.deswater.com

doi:10.5004/dwt.2019.23896

148 (2019) 248–258
April

# Cr(VI) reduction and adsorption by amino-functionalized magnetic loofah fiber composites

Cheng Liang, Chen Liu, Chunjie Yan*, Sen Zhou*

*Engineering Research Center of Nano-Geomaterials of Ministry of Education, Faculty of Materials Science and Chemistry, China, University of Geosciences, 388 Lumo Road, Wuhan 430074, China, email: 240764259@qq.com (C. Liang), 498403587@qq.com (C. Liu), Tel. /Fax + 86 15827484242, email: chjyan2005@126.com (C. Yan), zhousen@cug.edu.cn (S. Zhou)*

Received 26 April 2018; Accepted 1 February 2019

**ABSTRACT**

In this study, easily separable magnetic loofah fiber (AF-MLF) bio-adsorbent was prepared by surface modification with aminofunctional groups for Cr(VI) adsorption. This AF-MLF adsorbent could reduce partial Cr(VI) to nontoxic Cr(III)based on electron-donor effect of hydroxyl groups, so as to significantly reduce disposal difficulty of the spent adsorbents. Kinetic data and isotherms were conducted by a batch experiment. The kinetic analysis revealed that adsorption followed the pseudo-second-order model. The equilibrium data showed that Cr(VI) adsorption fitted with the Langmuir model, and the maximum adsorption capacity was 390.47 mg/g. Furthermore, various characterization methods, such as VSM, SEM, FT-IR, and XPS, were performed to elucidate the adsorption mechanism. The results from this study demonstrated that the AF-MLF is a highly efficient, low-priced and useful bio-adsorbent for chromium containing wastewater treatment.

*Keywords:* Magnetic loofah fiber; Amine-functionalized; Cr(VI); Adsorption; Reduction

## 1. Introduction

Hexavalent chromium (Cr(VI)), most of which exists in industrial wastewater, is a well-recognized potential genotoxic carcinogen, mutagen, and teratogen [1–3]. The World Health Organization had established an reference dose of 0.05 mg/L [3,4], 0.1 mg/L [4] and 0.2 mg/L [5] for Cr(VI) in potable water, inland surface water and industrial wastewater. Despite the current considerable reduction in chromium industry disposal, Cr(VI) is still frequently found in groundwater and various types of wastewater [6,7]. Hence, it is imperative to find appropriate treatments for the removal of Cr(VI) from aqueous solutions before discharging it into the environment.

In the past decades, various developed physicochemical methods have been studied to reduce the pollution of Cr(VI), such as adsorption, electrodialysis, membrane process, solvent extraction and chemical redox followed by precipitation [8–11]. Among these methods, adsorption based on electrostatic interaction is the most effective method owing to its high efficiency, easy operation process and complete removal of metal ions even at low concentrations [5,12,13]. However, the key of adsorption is the innocuous and efficient disposal of the spent adsorbent, namely, to reduce the toxic residual secondary pollution and separate the spent adsorbent from wastewater [14,15]. Recently, a breakthrough in the field is the successful preparation of the magnetic adsorbents with both reductive and adsorption properties [16]. Cr(VI) ions were enriched on the surface of anchoring magnetic iron oxide adsorbent and some of them were adsorbed while others were reduced, and then immobilized in the form of nontoxic trivalent chromium Cr(III) [6,17] in the adsorption process. At last, the spent magnetic adsorbent is separated by an external magnetic field.

In general, a number of adsorbents, including clay materials, fibrous materials, ion-exchange resin, activated carbon and carbon nanotubes, can be used for adsorption process. Ion-exchange resin is one of the most commonly adsorbent products in the commerce. But it still has certain disadvantages like high costs and being produced with unsustainable

*Corresponding author.

fossil raw material [18–20]. Consequently, many investigators have studied the feasibility of low-cost and environmentally friendly adsorbents. Nowadays, common agricultural waste materials have been given great attention to be used as adsorbents [21–23]. Jiang et al. [24] reported that biological adsorbent based on agricultural wasted husks that were fabricated by coating with polydopamine–polyethylenimine had certain adsorption capacity. Loofah fiber (LF) is a hydrophilic agricultural waste with a highly multimodal hierarchical porous structure of interconnecting pores which abundantly grown in many countries [25]. LF is mainly composed of 60% cellulose, 30% hemicellulose and 10% lignin, which can provide large amount of surface active hydroxyl functional groups [26,27]. Therefore, LF and its application as a viable adsorbent material are essential for removing heavy metal ions from wastewater because its abundant resources, surface structure and chemical property.

In this work, the objectives were to decrease toxic secondary pollution, to reduce disposal difficulty of the spent adsorbents (facilitate separation in the aquatic medium) and to increase Cr(VI) adsorption capacity using agricultural waste as the base. Therefore, a low-cost and renewable magnetic adsorbent was designed by coating with $Fe_3O_4$ nanoparticles and functionalized with amine groups. The obtained amine-functionalized magnetic LF (AF-MLF) exhibited high adsorption capacity and could be rapidly separated after adsorption. This property had greatly reduced disposal difficulty of the spent adsorbents. Meanwhile, some of Cr(VI) ions could be reduced to Cr(III) by AF-MLF during adsorption process of Cr(VI). Hence, the toxic secondary pollution was greatly decreased in this process. The adsorption kinetic was evaluated using the pseudo-first-order and pseudo-second-order models. The equilibrium isotherms of Cr(VI) were investigated by Langmuir and Freundlich models. Morphology, structures and physicochemical characteristics were also confirmed by SEM and FT-IR spectroscopy. Furthermore, the adsorption mechanism was analyzed by XPS.

## 2. Experimental section

### 2.1. Chemicals and materials

The LF used in the present investigation was collected from local countryside, Hubei Province, southern China, crushed into particles (20~40 mesh) after water washing and drying. Potassium dichromate ($K_2Cr_2O_7$), ferrous sulfate heptahydrate ($FeSO_4{\cdot}7H_2O$), epichlorohydrin (ECH), Ferric chloride hexahydrate ($FeCl_3{\cdot}6H_2O$), ethylenediamine (EDA), triethylamine (TEA) and N′N-dimethylformamide (DMF, >99%) were all analytical grade.

### 2.2. Preparation

Magnetic loofah fiber (MLF) was synthesized by chemical co-precipitation method. $FeCl_3{\cdot}6H_2O$ (9 mmol) and $FeSO_4{\cdot}7H_2O$ (6 mmol) were dissolved in 40 ml of deionized water and mixed with 2.5 g loofah fiber. Ammonia solution (10 wt%) was then added after vigorous stirring with ultrasound shaking for 30 min. The resulting dispersion was continuously stirred for 3 h at room temperature. The obtained solid (MLF) were washed with deionized water for several times until pH value was neutrality before drying for 3 h.

Then, the resultant MLF was modified by amination in which DMF was used as solvent. At first, ECH was chemically bonded to cellulose chains as an etherifying agent, producing epoxy cellulose ether. Second, epoxy cellulose ether chemically reacted with EDA. Last, the EDA-crosslinked ether was used as a bridge for the subsequent graft reaction with TEA. Typically, two grams of MLF reacted with 32 mL ECH and 96 mL DMF in a 250 mL three-neck flask equipped with a stirrer and a thermometer by water bathe at 85°C for 1 h. 12 mL of EDA was added and the mixture was stirred for 1 h at 85°C, followed by adding 24 mL of TEA for grafting and stirring for 2 h at 85°C. The solid was washed with 500 mL of distilled water, dried at 60°C for 5 h.

### 2.3. Characterization

The surface morphology and energy dispersive X-ray spectroscopy of samples were observed by scanning electron microscopy (SEM, SU8010, Hitachi, Ltd., Japan) with an energy dispersive X-ray spectroscopy (EDS, Oxford Instruments Link ISIS). The functional groups were investigated by FT-IR (Nicolet iS50, Thermo Fisher Scientific Inc., America), where the spectra were performed by ATR (Attenuated Total Reflection) and recorded from 4000 to 400 $cm^{-1}$. X-ray photoelectron spectrometer (VG Multilab2G Multilab2000) was used in the surface analysis.

### 2.4. Adsorption studies

The Cr(VI) adsorption properties were primarily evaluated by using a batch adsorption experiment, including the effect of pH, adsorption kinetics and adsorption isotherm. The general adsorption process was as follows: 20 mg of synthesized adsorbent mix with 20 mL Cr(VI) solution and shaken at 200 rpm for 12 h. Initial pH (2–8) of solution was adjusted by 0.1 M NaOH or HCl solution. The adsorption isotherms were obtained by different Cr(VI) concentrations from 0 to500 mg/L at 303.15, 313.15 and 323.15 K. The adsorption kinetics was conducted at regular intervals with Cr(VI) concentration of 200, 300 and 400 mg/L. In adsorption isotherms and kinetics study, each data point was conducted in different flask, so no correction was needed because of withdrawal of sampling volume. The change of Cr(VI) concentration was detected by an UV-visible spectrophotometer (model UV754GD, Shanghai). The absorbance was measured at λ = 540 nm. The adsorption amount is calculated by the following equation:

$$q_e = (C_0 - C_e)\frac{V}{m} \tag{1}$$

where $q_e$ (mg/g) is the equilibrium adsorption capacity, $C_0$ (mg/L) and $C_e$ (mg/L) are the initial and equilibrium concentration, respectively. $V$ (L) and $m$ (g) are the volume of solutions and the mass of the adsorbent.

### 2.5. Theory

Adsorption kinetic is one of the most important characteristics that represent the adsorption efficiency and poten-

tial applications of the adsorbent, as it provides valuable information on the reaction pathways and in the mechanism of adsorption reaction. In order to elucidate the adsorption kinetic process, three of the most important kinetic models (the pseudo-first-order, pseudo-second-order model and Elovich equation) employed in this work were summarized as follows [28–30]:

The kinetic model of the pseudo-first-order assumes that the adsorption rate is a function of the adsorption capacity as shown in Eq. (2):

$$q_t = q_e(1 - e^{-k_1 t}) \tag{2}$$

On the basis of pseudo-second-order kinetic model, the adsorption mechanism can be explained as chemisorption. The expression of this model is expressed in the form (3):

$$q_t = \frac{k_2 q_e^2 t}{(1 + k_2 q_e t)} \tag{3}$$

Elovich equation is another rate equation based on the overall adsorption process. The equations are presented by Eq. (4):

$$q_t = [\ln(\alpha\beta t + 1)] / \beta \tag{4}$$

where $q_t$ (mg/g) and $t$ (min) are the adsorption capacity within time t and contact time. $k_1$ (min$^{-1}$), $k_2$ (g·mg$^{-1}$·min$^{-1}$), α (mg/g min) and β (g/mg) are the rate of pseudo first order adsorption, pseudo second-order, initial adsorption rate and desorption constant respectively.

Furthermore, the Weber-Morris diffusion model was used to evaluating the rate-limiting step [31].

$$q_t = k_i t^{0.5} + I \tag{5}$$

Both $k_i$ (mg·g$^{-1}$·min$^{-1/2}$) and $I$ (mg/g) are the Weber-Morris diffusion constants.

Adsorption isotherms are important requirements for adsorption system. Furthermore, it is crucial to have a good estimate of the adsorption capacity of the adsorbent for application. A wide variety of equilibrium isotherm models (Langmuir, Freundlich, Toth, Redlich–Peterson, Sips, Temkin, Dubinin–Radushkevich) have been chosen to evaluate the equilibrium results. The isotherm models equations are as follows [32–35]:

$$q_e = \frac{q_m K_L C_e}{1 + K_L C_e} \quad \text{Langmuir} \tag{6}$$

$$q_e = K_F C_e^{1/n} \quad \text{Freundlich} \tag{7}$$

$$q_e = \frac{K_t C_e}{(a_t + C_e)^{\frac{1}{n_t}}} \quad \text{Toth} \tag{8}$$

$$q_e = \frac{K_R C_e}{1 + a_R C_e^{\beta}} \quad \text{Redlich-Peterson} \tag{9}$$

$$q_e = \frac{K_{LF} C_e}{1 + a_{LF} C_e^{n_R}} \quad \text{Sips or Langmuir-Freundlich} \tag{10}$$

$$q_e = \frac{RT}{K_T} \ln(n_t C_e) \quad \text{Temkin isotherm} \tag{11}$$

$$q_e = K_{DR} \exp\{-n_{DR}[\mathrm{RT}\ln(1 + \tfrac{1}{C_e})]^2\} \quad \text{Dubinin-Radushkevich isotherm} \tag{12}$$

where $C_e$ is the equilibrium concentration of Cr(VI) (mg/L), $q_e$ is equilibrium adsorption capacity (mg/g). The detailed parameters are listed in Table 3.

## 3. Results and discussion

### 3.1. Characterization

#### 3.1.1. VSM of AF-MLF

Fig. 1 shows the curve of magnetism of AF-MLF obtained via vibrating sample magnetometer (VSM) at room temperature. The curve shows that AF-MLF have a reversible hysteresis behavior and the magnetization saturation value are 7.3 emu/g. The results suggest that the AF-MLF can be effectively separated easily from solution by applying an external magnetic field.

#### 3.1.2. FT-IR of AF-MLF

FT-IR spectra of LF, AF-MLF, LF after adsorption and AF-MLF after adsorption are shown in Fig. 2. Compare with Fig. 2a, Fig. 2b appears some new absorption bands. The new bands at 1328 cm$^{-1}$, 1649 cm$^{-1}$, 1560 cm$^{-1}$, 605 cm$^{-1}$ can be attributed to C–N, C=O [36,37], N–H [38,39] and chloralkane or Fe–O vibration [36,38,40], respectively. In addition, a strong broad band is located at 3402 cm$^{-1}$, which can be assigned to the overlap of O–H and N–H [36,39]. The appearance of new bands successfully indicates that a large number of amine functional groups are appeared on the surface of AF-MLF. For FTIR spectrum of AF-MLF after adsorption (Fig. 2c), two new bands appearing at around 1,600 and 1,400 cm$^{-1}$ [41] suggest that chromium is adsorbed.

#### 3.1.3. SEM and EDS of AF-MLF

Fig. 3 shows the SEM and the corresponding EDS images of samples. It appears that the surface morphologies of LF and AF-MLF are obviously different, and the surface morphologies of LF and AF-MLF almost unchanged after Cr(VI) adsorption. Comparing to the surface morphologies of LF (Figs. 3a and a$_1$), it is found that AF-MLF (Figs. 3b and

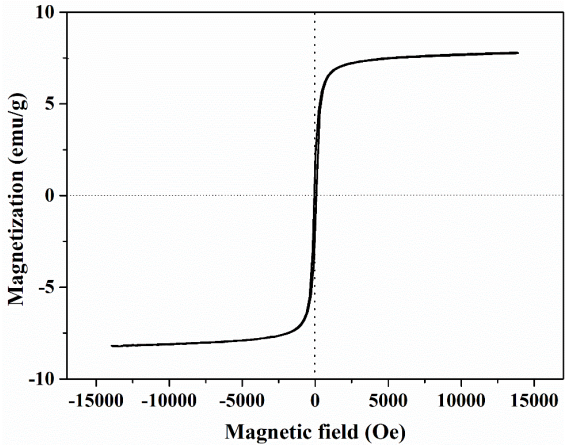


Fig. 1. Magnetization curves of the AF-MLF.

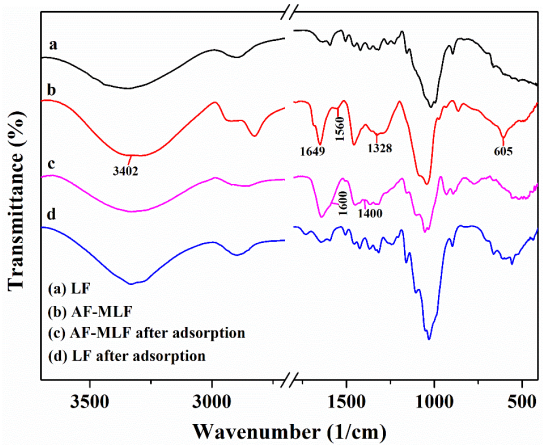


Fig. 2. FITR spectra of LF (a), AF-MLF (b), AF-MLF after adsorption (c) and LF after adsorption (d).

$b_1$) is covered by abundant clear and uniform smooth polymer protuberances after the combination with cross-linked chemicals, indicating the successful increase of surface contact area and active sites, thus improving adsorption capacity [42,43]. Combining with the EDS map scanning, the appearance of Fe, N, Cl confirms the success of the modification by aminofunctional groups and the coating by $Fe_3O_4$. After adsorption, the elements chromium appears on the surface of LF and AF-MLF and the atomic proportion of N and Cr is approximately 1: 1 which proves that the main adsorption occurs between the protonated quaternary ammonium nitrogen/$-N^+$ and $HCrO_4^-$.

### 3.2. pH and zeta potential

The initial pH values can significant affect the adsorption capacity because the forms of the chromium species in solution are different. The Cr(VI) adsorption behavior by LF

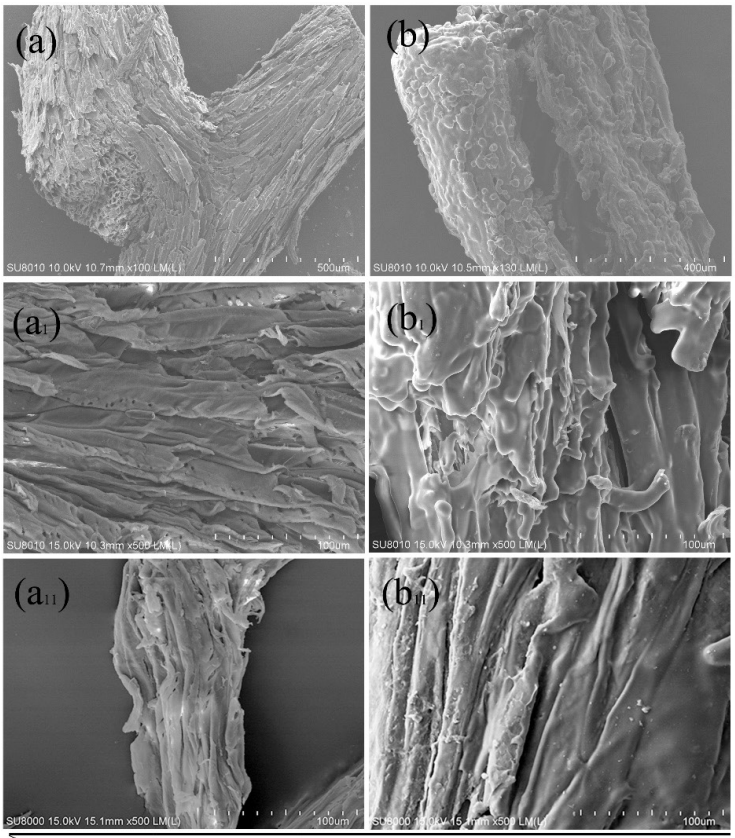


| Wt% / Element | LF /before | LF /after | AF-MLF /before | AF-MLF /after |
|---|---|---|---|---|
| CK | 45.96 | 46.15 | 36.15 | 29.79 |
| OK | 54.04 | 53.73 | 43.12 | 35.21 |
| FeK | \ | \ | 14.58 | 12.07 |
| ClK | \ | \ | 01.04 | \ |
| NK | \ | \ | 05.11 | 4.43 |
| CrK | \ | 0.12 | \ | 18.50 |

Fig. 3. SEM/EDS analysis of LF before adsorption (a, $a_1$), LF after adsorption ($a_2$), AF-MLF before adsorption (b, $b_1$) and AF-MLF after adsorption ($b_2$).

and AF-ML Funder different pH conditions (2–8) is shown in Fig. 4. It is obvious that the maximum adsorption capacity is 344.4 mg/g at pH = 2, about 20 times higher than that of LF and the isoelectric point of the adsorbent is 7.6 which is higher than that of other modified biomass adsorbent [34,35]. The adsorption capacity of Cr(VI) by AF-MLF decrease gradually along with pH increasing. This result shows the same trend with the change of ZP values, illustrates that the positively charged quaternary ammonium groups are successfully grafted on the surface of LF and demonstrates that Cr(VI) can diffuse into the surface adsorption sites of AF-MLF by electrostatic attraction. The positive electrical property of AF-MLF decreases with the increases of pH value, and electrostatic attractions are therefore weak [44].

Moreover, the different existing forms of Cr(VI) in aqueous solution can significant affect the adsorption. $HCrO_4^-$ is the mainly existing form when pH < 3. While in higher pH, the existing forms are mainly $CrO_4^{2-}$ and $Cr_2O_7^{2-}$. Obviously, $HCrO_4^-$ ions only correspond to one active adsorption site [45]. As a result, AF-MLF had stronger adsorption capacity for Cr(VI) under pH < 3.

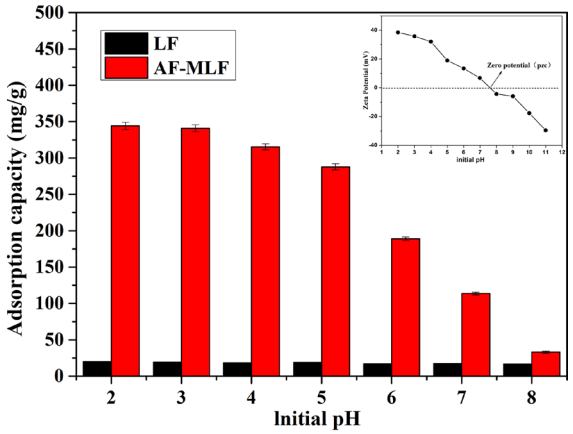


Fig. 4. Effect of initial solution pH on the adsorption of Cr(VI) [dosage: 1 g/L; T = 25°C; shaking speed: 250 r/min; solution concentrations: 400 mg/L; contacting time: 12 h] and zeta potential of AF-MLF.

### 3.3. Kinetic study

Fig. 5a is adsorption kinetics of AF-MLF. It can be observed that the adsorption capacity of AF-MLF increases fast in the first 25 min during adsorption process which could reach about 70% of maximum adsorption capacity. This is probably because the surface of AF-MLF could provide sufficient active sites for Cr(VI) adsorption at the initial period of adsorption. Thereafter, excessive amount of surface adhere chromium may cause the trend of slow growth for adsorption capacity due to electrostatic repulsion.

The pseudo-first-order, pseudo-second-order and Elovich models (see Fig. 5a) are applied to estimate the adsorption reaction rate and derive the adsorption mechanism. The kinetic parameters are summarized in Table 1. The theoretical calculated values agree well with the experimental values and the correlation coefficient value $R^2$ is nearly 1.0, indicating the applicability of pseudo-second-order model. For the Elovich results in Table 1, the wide variety of α indicates the inadequacy of the Elovich model for the chromium removal.

The actual rate-controlling step (based on Weber-Morris model) in adsorption process is further analyzed. It can be seen that the data points of Cr(VI) adsorption under different initial concentrations are formatted by three straight lines. The first linear portion has a steeper slope. It may indicate that the main rate-controlling step of first stage is outer or film diffusion. This process refers to Cr(VI) is transported from solution to the boundary layer of AF-MLF particles or the external surface of the composite. The second lower slope portion represents the gradual adsorption stage, which indicates that the rate-controlling step is intraparticle or pore diffusion. Finally, diffusion has been to slow and then reach the equilibrium. The root cause of this phenomenon is extremely low solute concentration, considerably few available amine groups, increasingly thick boundary layer and soon. The diffusion-based (Weber-Morris) model parameters are shown in Table 2. Obviously, the values of the fitting parameters in three initial concentrations had the same results: $k_{i,1} > k_{i,2} > k_{i,3}$. Therefore, these results suggest that the overall adsorption process may be of a complex nature. The rate-determining step in initial stage is film diffusion, followed is slow intraparticle diffusion.

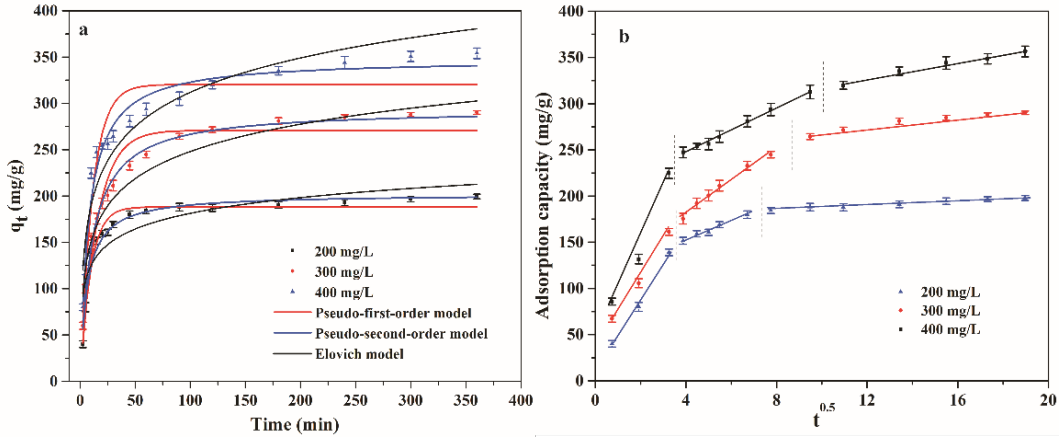


Fig. 5. (a) Pseudo-first-order and pseudo-second-order models, (b) plots of Weber–Morris diffusion model for the kinetics data [dosage: 1 g/L; T = 25°C; pH = 2; shaking speed: 250 r/min; contacting time: 12 h].

Table 1
Coefficients of pseudo-first-order and pseudo-second-order adsorption kinetic models

| Adsorption kinetic models | Parameters | Initial concentrations | | |
|---|---|---|---|---|
| | | 200 mg/L | 300 mg/L | 400 mg/L |
| Pseudo-first-order model | $q_{e,exp}$ (mg/g) | 199.51 | 292.17 | 361.04 |
| | $k_1$ (/min) | 0.1068 | 0.0658 | 0.0898 |
| | $q_{e,cal}$ (mg/g) | 188.02 | 270.83 | 320.28 |
| | $R^2$ | 0.9379 | 0.9361 | 0.8945 |
| Pseudo-second-order model | $k_2$ (g/(mg·min)) | 0.0007933 | 0.0003293 | 0.0003685 |
| | $q_{e,cal}$ (mg/g) | 202.12 | 294.07 | 348.03 |
| | $R^2$ | 0.9719 | 0.9943 | 0.9685 |
| Elovich model | α (mg/(g·min)) | 403.7222 | 143.5724 | 179.513 |
| | β (g/mg) | 0.04086 | 0.02348 | 0.01865 |
| | $R^2$ | 0.7725 | 0.9414 | 0.9073 |

Table 2
Kinetic parameters calculated from Weber–Morris model for Cr(VI) adsorption

| Diffusion model | Parameters | Initial concentrations | | |
|---|---|---|---|---|
| | | 200 mg/L | 300 mg/L | 400 mg/L |
| First stage | $k_{i,1}$ (mg/(g ·min$^{0.5}$)) | 30.15 | 34.40 | 39.92 |
| | $I_1$ (mg/g) | 25.10 | 42.26 | 54.14 |
| | $R^2$ | 0.9986 | 0.9910 | 0.9774 |
| Second stage | $k_{i,2}$ (mg/(g ·min$^{0.5}$)) | 9.17 | 12.69 | 12.99 |
| | $I_2$ (mg/g) | 117.05 | 111.41 | 199.45 |
| | $R^2$ | 0.9797 | 0.9804 | 0.9944 |
| Three stage | $k_{i,3}$ (mg/(g ·min$^{0.5}$)) | 1.16 | 2.66 | 4.37 |
| | $I_2$ (mg/g) | 176.15 | 242.03 | 274.18 |
| | $R^2$ | 0.9640 | 0.9330 | 0.9709 |

### 3.4. Adsorption isotherms

Adsorption isotherms by AF-MLF at different temperatures are shown in Fig. 6. It can be seen that the Cr(VI) absorption capacities increase quickly at first with the increasing of equilibrium concentration. This might attribute to the sufficient surface-active sites when relatively initial Cr(VI) concentration is not high in adsorption process. In this study, the equilibrium data is evaluated by seven different isotherms models.

The fitting curves are shown in Fig. 6, and the detailed equations are listed in Table 3 together with the best fitted values of the parameters. Through a comparison between $R^2$ values of seven isotherms, meanwhile, analyzing the fitting results and experimental data, it is found that Sips or Langmuir–Freundlich, Langmuir, Redlich-Peterson and Toth models are suitable to describe the adsorption isotherm. The Langmuir–Freundlich and Langmuir models indicate that monolayer adsorption is predominant in the adsorption and the surface-active adsorption sites are uniformly distributed on the surface of AF-MLF. The Redlich-Peterson and Toth isotherm also fit well with experimental data. It can be seen that the values of parameter β tend to unity and parameter $n_t$ is near 1, that is the isotherms are approaching the Langmuir form.

The Langmuir parameters $Q_{max}$ and $K_L$ increase with increasing of temperature, which indicates that the Cr(VI) adsorption is endothermic reaction. The saturated adsorption capacity calculate is 390.47 mg/g. Comparing to several reported bioadsorbents list in Table 4, it is found that the AF-MLF should be a better choice among them.

### 3.5. Adsorption mechanism

To investigate Cr(VI) removal mechanism, XPS is used to characterize the surface elements and its distribution of valence state. The XPS wide scan spectrum of LF and modified LF are shown in Fig. 7a. After modifying, the content of nitrogen obviously is increased which indicate that amino functional groups have been successfully grafted. Meanwhile, some new peaks appear around the binding energies of 197 eV and 710 eV which fit well to the photoelectron spectra of Cl 2p and Fe 2p, respectively. This indicates that $Fe_3O_4$ magnetic nanoparticles exist in the composite and the surface functional group structure of

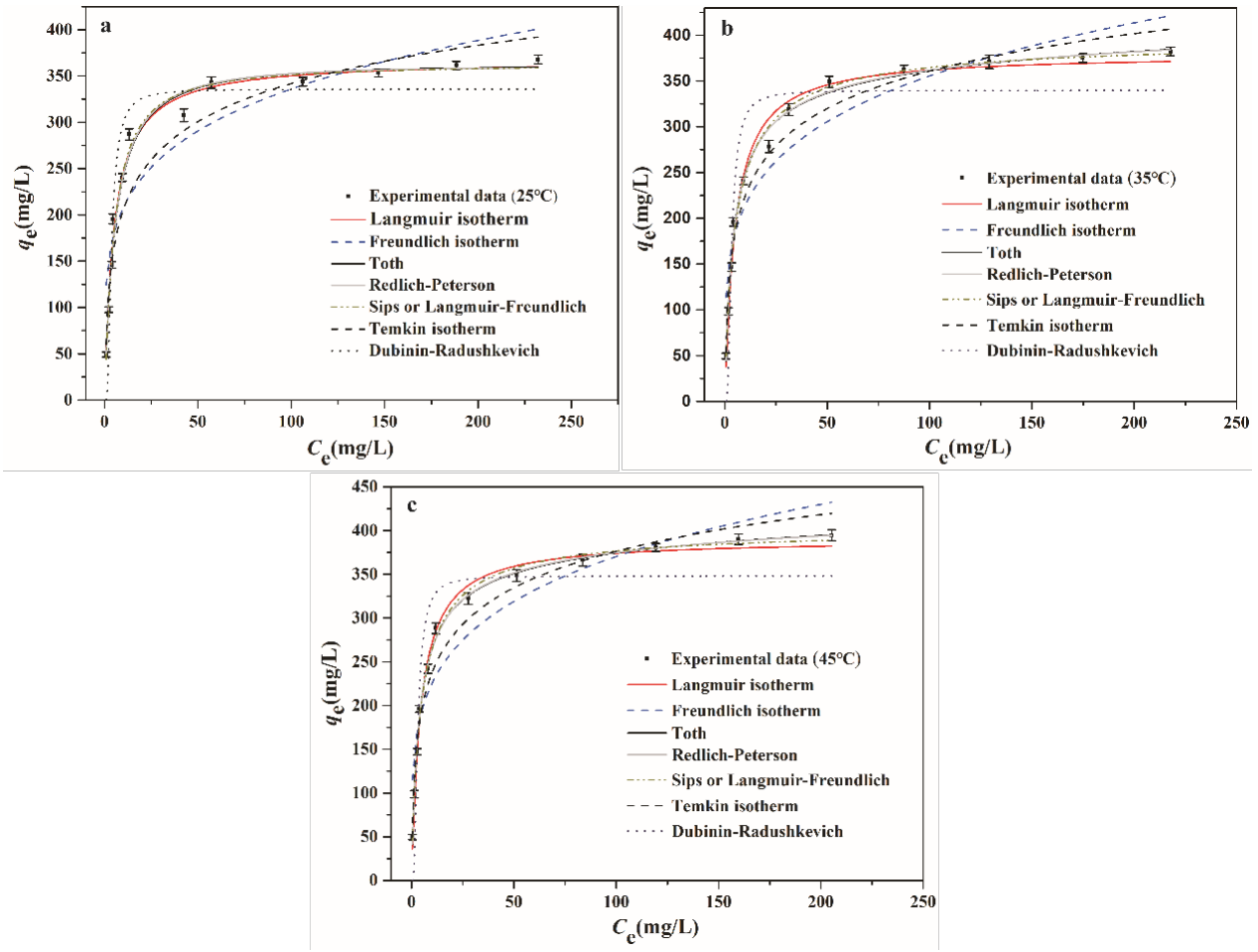


Fig. 6. Adsorption equilibrium data of Cr(VI) onto AF-MLF [dosage: 1 g/L; pH = 2; shaking speed: 250 r/min; contacting time: 12 h] fitting to seven isotherm equations.

anion adsorbent AF-MLF is similar to commercial resin:–$N^+R_3$ $Cl^-$ [53,54].

Analyses XPSwide scan spectrum of Cr(VI) adsorbed at AF-MLF, it can easily find the absorption band of Cl 2p tends to vanish and the characteristic peak of Cr2p around the binding energies of 580 eV appears (see Fig. 7a). This shows that the few partial adsorption process is conducted by ion exchange between Cr(VI) and $Cl^-$ ions. The detailed XPS spectrum of Cr 2p region is shown in Fig. 7b which have two peaks Cr2p1/2 (586.2 eV) and Cr 2p3/2 (576.45 eV). This confirm that Cr(III) is presented on the surface of AF-MLF after adsorption [55]. Through XPS analysis, the broad peak of Cr 2p3/2 can be fitted with two peaks at binding energies of 576.1 ± 0.1 eV and 578.5 ±0.1, which are characteristics of Cr(III)-OH and Cr(VI)–O in $HCrO_4^-$ species, respectively. These results demonstrate that partial Cr(VI) have been reduced to nontoxic Cr(III), and Cr(III) can be adsorbed by AF-MLF. It is probably because Cr(III) is anion metal ions and can be chelated with surface carboxyl and hydroxyl groups.

To further investigate the uptake mechanism, we explore the XPS spectra of N 1s and O 1s. The peak of N 1s can be fitted with two peaks at binding energies of 399.0 and 400.8 eV (see Figs. 7c and d), which are the characteristics of amino nitrogen/–NH species and quaternary ammonium nitrogen/$–N^+$, respectively [38]. Through compare and analyze the XPS spectra before and after Cr(VI) adsorption, it can be found that the relative peak area of quaternary ammonium nitrogen/$–N^+$ is significantly reduced after Cr(VI) adsorption, and the ratio of –NH/$–N^+$ decrease from 0.51 to 0.03. This confirms that the quaternary ammonium nitrogen/$–N^+$ play a major role in adsorption process. Fitting of the XPS O1s spectra (see Figs. 7e and f), an assignment of peaks can be obtained. The peak at 531.69 eV correspond to C–OH and $Cr(OH)_3$, at 531.1 eV correspond to C–O–C, at 529.6 eV corresponds to Fe–O, at 530.5 eV corresponds to C=O and $CrO_3$. It can easily find that the peak of C–H is reduced while some new peaks of C=O, $CrO_3$, and $Cr(OH)_3$ appear after adsorption. The appearance of C=O peak is probably due to the oxidation of the –OH groups, implying that the –OH groups are the electron donor in reduction.

In conclusion, the adsorption mechanism of AF-MLF on Cr(VI) can be divided into the following stages. Firstly, electrostatic attraction makes the Cr(VI) transfer from solution to the surface of adsorbent, and then Cr(VI) enrich on the surface by ion exchange processes between $–N^+$ and Cr(VI). Subsequently, some of Cr(VI) ions are reduced to Cr(III)

Table 3
Adsorption isotherm constants for Cr(VI) adsorption

| Adsorption isotherm constants | Parameters | 25°C | 35°C | 45°C |
|---|---|---|---|---|
| Langmuir | $q_{max}$ (mg/g) | 367.78 | 379.65 | 390.47 |
| | $K_L$ (L/mg) | 0.1991 | 0.2039 | 0.2292 |
| | $R^2$ | 0.9832 | 0.9851 | 0.9917 |
| Freundlich | $K_F$ ((mg/g)/(mg/L)$^{1/n}$) | 128.23 | 129.98 | 137.38 |
| | $1/n$ (mg/L) | 0.2091 | 0.2185 | 0.2154 |
| | $R^2$ | 0.8401 | 0.8913 | 0.8204 |
| Toth | $K_t$ (L/g) | 402.77 | 284.35 | 300.07 |
| | $a_t$ (L/mg) | 5.9501 | 3.2720 | 3.0294 |
| | $n_t$ | 0.9841 | 1.0623 | 1.0574 |
| | $R^2$ | 0.9903 | 0.9938 | 0.9949 |
| Redlich-Peterson | $K_R$ (L/g) | 64.425 | 97.313 | 109.45 |
| | $a_R$ (1/mg) | 0.1591 | 0.3280 | 0.3500 |
| | β | 1.0178 | 0.9486 | 0.9530 |
| | $R^2$ | 0.9904 | 0.9939 | 0.9950 |
| Sips or Langmuir-Freundlich | $K_{LF}$ (L/g) | 58.948 | 94.528 | 105.41 |
| | $n_{LF}$ | 1.1645 | 0.8379 | 0.8612 |
| | $a_{LF}$ (L/mg) | 0.1959 | 0.1803 | 0.2100 |
| | $R^2$ | 0.9916 | 0.9938 | 0.9949 |
| Temkin isotherm | $K_T$ | 18.107 | 18.874 | 19.064 |
| | $n_T$ (L/mg) | 3.1450 | 4.5566 | 5.1674 |
| | $R^2$ | 0.9580 | 0.9780 | 0.9791 |
| Dubinin-Radushkevich isotherm | $K_{DR}$ (mg/g) | 335.78 | 339.79 | 348.16 |
| | $n_{DR}$ (mol$^2$/kJ$^2$) | 1.095E-5 | 8.059E-6 | 7.057E-6 |
| | $R^2$ | 0.9137 | 0.8714 | 0.8755 |

Table 4
Maximum adsorption capacities for the adsorption of Cr(VI) onto various biomass adsorbents

| Adsorbents | Adsorption capacity (mg/g) | Conditions (pH values) | Refs. |
|---|---|---|---|
| Modified banana skin | 249.6 | 1.5 | [46] |
| Composite chitosan | 153.8 | 4.0 | [47] |
| Modified wheat straw | 322.6 | 4.7 | [48] |
| Wheat bran | 310.58 | 2.0 | [49] |
| Wheat straw amphoteric adsorbent | 227.3 | 4.19 | [50] |
| Thermally activated weed | 247 | 1.7 | [51] |
| graphene oxide coated biochar composite | 150.02 | 2.0 | [52] |
| LF | 20.12 | 2.0 | This work |
| AF-MLF | 390.47 | 3.0 | This work |

based on electron-donor effect of –OH group. Finally, Cr(III) is attached on the surface of the adsorbent by chelation.

### 3.6. Desorption-adsorption studies

In this study, the desorption of Cr(VI) ions are performed by using 0.1 mol/L NaOH solution and AF-MLF are collected by an external magnet. Fig. 8 shows the adsorption capacity of AF-MLF in function of the adsorption-desorption cycles of Cr(VI) ions. After three cycles, the adsorption capacity of AF-MLF remains almost 130.81 mg/g, which is higher than that of previously reported magnetic adsorbents [56]. Nevertheless, the regeneration performance of AF-MLF still requires further study and deeper improvement.

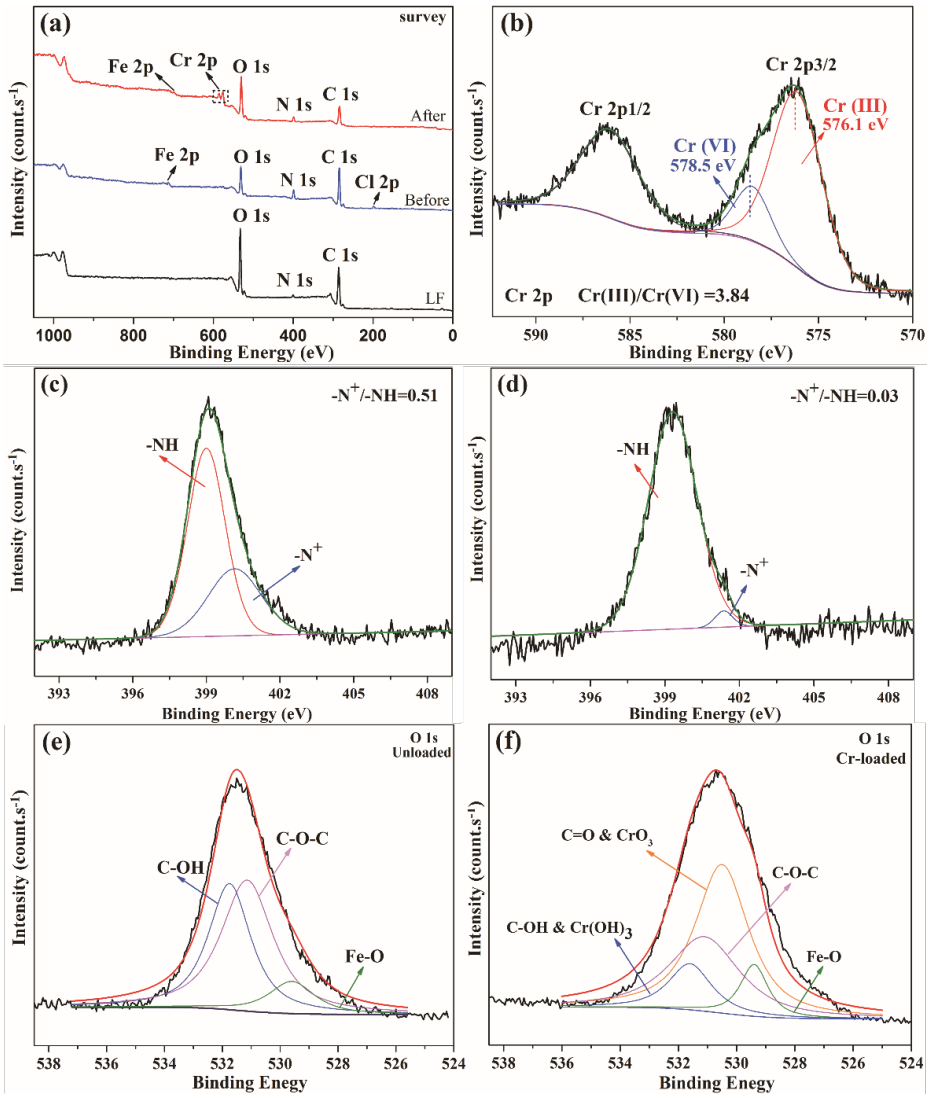


Fig. 7. (a) XPS wide scan spectra of the LF and AF-MLF, (b) XPS spectra of Cr 2p, (c) and (d) XPS spectra of N 1s before and after adsorption, (e) and (f) XPS spectra of O 1s before and after adsorption.

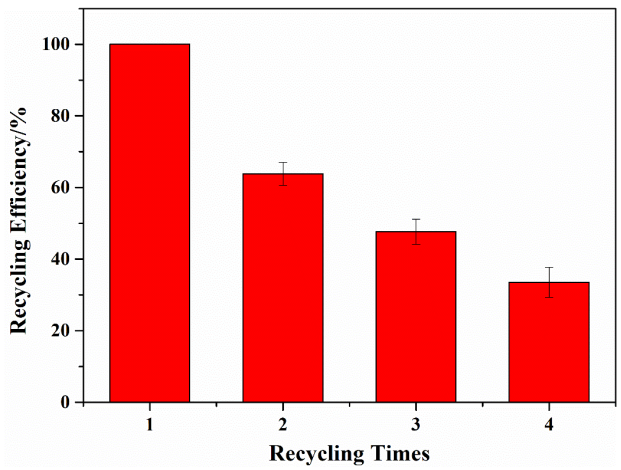


Fig. 8. Sorption–desorption cycles for AF-MLF.

## 4. Conclusions

AF-MLF was successfully synthesized through surface modification with aminofunctional groups. This adsorbent had easy solid-liquid separation characteristic and could be easily separated by a magnetic field. The maximum adsorption capacity of Cr(VI) that was calculated based on Langmuir model and the maximum adsorption was 390.47 mg/g. This value was higher than the other reported adsorbents. The result confirmed that AF-MLF was a highly efficient and useful adsorbent for chromium containing wastewater treatment. XPS and zeta potential indicated that the adsorption mechanism between Cr(VI) and AF-MLF referred to electrostatic attraction, ion exchange and chelation. XPS shows that some of Cr(VI) ions was reduced to Cr(III) based on electron-donor effect of –OH group. Moreover, the kinetics of adsorption revealed that the adsorption process involved physical acting and chemical bonding. The equilibrium isotherm described the Cr(VI) adsorption well.

**Acknowledgements**

This work was supported by National Key R&D Program of China (No: 2017YFB0310805) and Funding of Engineering Research Center of Nano-Geo Materials of Ministry of Education, China University of Geosciences (NGM2017KF006).

**References**

[1] B.A. Butruk-Raszeja, P.A. Trzaskowska, A. Kuźminska, T. Ciach, Polyurethane modification with acrylic acid by Ce(IV)-initiated graft polymerization, Open Chem., 14 (2016) 206–214.
[2] L. Dupont, E. Guillon, Removal of hexavalent chromium with a lignocellulosic substrate extracted from wheat bran, Environ. Sci. Technol., 37 (2003) 4235–4241.
[3] W. Qi, Y. Zhao, X. Zheng, M. Ji, Z. Zhang, Adsorption behavior and mechanism of Cr(VI) using Sakura waste from aqueous solution, Appl. Surf. Sci., 360 (2016) 470–476.
[4] T.S. Anirudhan, J. Nima, P.L. Divya, Adsorption of chromium(VI) from aqueous solutions by glycidylmethacrylate-grafted-densified cellulose with quaternary ammonium groups, Appl. Surf. Sci., 279 (2013) 441–449.
[5] J. Sun, Z. Zhang, J. Ji, M. Dou, F. Wang, Removal of $Cr^{6+}$ from wastewater via adsorption with high-specific-surface-area nitrogen-doped hierarchical porous carbon derived from silkworm cocoon, Appl. Surf. Sci., 405 (2017) 372–379.
[6] N. Zaitseva, V. Zaitsev, A. Walcarius, Chromium(VI) removal via reduction-sorption on bi-functional silica adsorbents, J. Hazard. Mater., 250–251 (2013) 454–461.
[7] J. Guertin, Toxicity and Health Effects of Chromium (all oxidation States), Chromium(VI) Handbook, 2004, pp. 213–232.
[8] P. Miretzky, A.F. Cirelli, Cr(VI) and Cr(III) removal from aqueous solution by raw and modified lignocellulosic materials: a review, J. Hazard. Mater., 180 (2010) 1–19.
[9] A.E. Pagana, S.D. Sklari, E.S. Kikkinides, V.T. Zaspalis, Combined adsorption–permeation membrane process for the removal of chromium (III) ions from contaminated water, J. Membr. Sci., 367 (2011) 319–324.
[10] J.W. Patterson, Industrial Wastewater Treatment Technology, 2nd ed., Ann Arbor Science, 1985.
[11] Y. Yan, Q. An, Z. Xiao, S. Zhai, B. Zhai, Z. Shi, Interior multi-cavity/surface engineering of alginate hydrogels with polyethylenimine for highly efficient chromium removal in batch and continuous aqueous systems, J. Mater. Chem. A, 5 (2017) 17073–17087.
[12] S. Babel, T.A. Kurniawan, Low-cost adsorbents for heavy metals uptake from contaminated water: a review, J. Hazard. Mater., 97 (2003) 219–243.
[13] T. Hao, C. Yang, X. Rao, J. Wang, C. Niu, X. Su, Facile additive-free synthesis of iron oxide nanoparticles for efficient adsorptive removal of Congo red and Cr(VI), Appl. Surf. Sci., 292 (2014) 174–180.
[14] D. Mohan, C.U. Pittman, Activated carbons and low cost adsorbents for remediation of tri- and hexavalent chromium from water, J. Hazard. Mater., 137 (2006) 762–811.
[15] H. Lin, S. Han, Y. Dong, Y. He, The surface characteristics of hyperbranched polyamide modified corncob and its adsorption property for Cr(VI), Appl. Surf. Sci., 412 (2017) 152–159.
[16] X.B. Fang, Z.Q. Fang, P.K.E. Tsang, W. Cheng, X.M. Yan, L.C. Zheng, Selective adsorption of Cr(VI) from aqueous solution by EDA-$Fe_3O_4$ nanoparticles prepared from steel pickling waste liquor, Appl. Surf. Sci., 314 (2014) 655–662.
[17] R.S. Karale, D.V. Wadkar, P.B. Nangare, Removal and recovery of hexavalent chromium from industrial waste water by precipitation with due consideration to cost optimization, J. Environ. Res. Develop., 2 (2007) 209–216.
[18] A. Dabrowski, Z. Hubicki, P. Podkoscielny, E. Robens, Selective removal of the heavy metal ions from waters and industrial wastewaters by ion-exchange method, Chemosphere, 56 (2004) 91–106.
[19] T. Yoshioka, Studies of polystyrene-based ion-exchange fiber. III. A novel fiber-form chelating exchanger and its adsorption properties for heavy-metal ions, B. Chem. Soc. JPN., 58 (1985) 2618–2625.
[20] H.S. Dong, Y.G. Ko, U.S. Choi, W.N. Kim, Design of high efficiency chelate fibers with an amine group to remove heavy metal ions and pH-related FT-IR analysis, Ind. Eng. Chem. Res., 43 (2004) 2060–2066.
[21] W. Song, B. Gao, X. Xu, F. Wang, N. Xue, S. Sun, W. Song, R. Jia, Adsorption of nitrate from aqueous solution by magnetic amine-crosslinked biopolymer based corn stalk and its chemical regeneration property, J. Hazard. Mater., 304 (2016) 280–290.
[22] F. Reguyal, A.K. Sarmah, W. Gao, Synthesis of magnetic biochar from pine sawdust via oxidative hydrolysis of $FeCl_2$ for the removal sulfamethoxazole from aqueous solution, J. Hazard. Mater., 321 (2017) 868–878.
[23] A. Witek-Krowiak, R.G. Szafran, S. Modelski, Biosorption of heavy metals from aqueous solutions onto peanut shell as a low-cost biosorbent, Desalination, 265 (2011) 126–134.
[24] X. Jiang, Q. An, Z. Xiao, S. Zhai, Z. Shi, Mussel-inspired surface modification of untreated wasted husks with stable polydopamine/polyethylenimine for efficient continuous Cr(VI) removal, Mater. Res. Bull., 102 (2018) 218–225.
[25] U. Tuncel, A. Turan, F. Markoc, Loofah sponge as an interface dressing material in negative pressure wound therapy: results of an in vivo study, Ostomy/wound Management, 60 (2014) 37–45.
[26] Y. Bulut, Z. Tez, Adsorption studies on ground shells of hazelnut and almond, J. Hazard. Mater., 149 (2007) 35–41.
[27] A. Altinisik, E. Gur, Y. Seki, A natural sorbent, luffa cylindrica for the removal of a model basic dye, J. Hazard. Mater., 179 (2010) 658–664.
[28] Y.S. Ho, G. Mckay, Pseudo-second order model for sorption processes, Process Biochem., 34 (1999) 451–465.
[29] Y.S. Ho, J.C.Y. Ng, G. McKay, Kinetics of pollutant sorption by biosorbents: review, Separ. Purif. Method., 29 (2011) 189–232.
[30] L.R. Martins, J.A.V. Rodrigues, O.F.H. Adarme, T.M.S. Melo, L.V.A. Gurgel, L.F. Gil, Optimization of cellulose and sugarcane bagasse oxidation: Application for adsorptive removal of crystal violet and auramine-O from aqueous solution, J. Colloid Interface Sci., 494 (2017) 223–241.
[31] G. Annadurai, R.S. Juang, D.J. Lee, Use of cellulose-based wastes for adsorption of dyes from aqueous solutions, J. Hazard. Mater., 92 (2002) 263–274.
[32] I.A.W. Tan, B.H. Hameed, A.L. Ahmad, Equilibrium and kinetic studies on basic dye adsorption by oil palm fibre activated carbon, Chem. Eng. J., 127 (2007) 111–119.
[33] O. Redlich, D. Peterson, L., A useful adsorption isotherm, J. Phys. Chem., 63 (1959) 1024–1024.
[34] P.C.C. Siu, L.F. Koong, J. Saleem, J. Barford, G. McKay, Equilibrium and kinetics of copper ions removal from wastewater by ion exchange, Chin. J. Chem. Eng., 24 (2016) 94–100.
[35] K.Y. Foo, B.H. Hameed, Insights into the modeling of adsorption isotherm systems, Chem. Eng. J., 156 (2010) 2–10.
[36] C.H. Yen, H.L. Lien, J.S. Chung, H.D. Yeh, Adsorption of precious metals in water by dendrimer modified magnetic nanoparticles, J. Hazard. Mater., 322 (2017) 215–222.
[37] T.H. Ha, J.Y. Jeong, B.H. Chung, Immobilization of hexa-arginine tagged esterase onto carboxylated gold nanoparticles, Chem. Commun., 31 (2005) 3959–3961.
[38] B. Pan, F. Gao, H. Gu, Dendrimer modified magnetite nanoparticles for protein immobilization, J. Colloid Interface Sci., 284 (2005) 1–6.
[39] Y. Jiang, Q. Gao, H. Yu, Y. Chen, F. Deng, Intensively competitive adsorption for heavy metal ions by PAMAM-SBA-15 and EDTA-PAMAM-SBA-15 inorganic–organic hybrid materials, Micropor. Mesopor. Mater., 103 (2007) 316–324.
[40] F. Gao, B. Pan, W. Zheng, L. Ao, H. Gu, Study of streptavidin coated onto PAMAM dendrimer modified magnetite nanoparticles, J. Magn. Magn. Mater., 293 (2005) 48–54.
[41] G. Nagpal, A. Bhattacharya, N.B. Singh, Removal of chromium(VI) from aqueous solution by carbon waste from thermal power plant, Desal. Water Treat., 57 (2015) 9765–9775.

[42] S. Deng, Y. Zheng, F. Xu, B. Wang, J. Huang, G. Yu, Highly efficient sorption of perfluorooctane sulfonate and perfluorooctanoate on a quaternized cotton prepared by atom transfer radical polymerization, Chem. Eng. J., 193–194 (2012) 154–160.
[43] S. Deng, L. Niu, Y. Bei, B. Wang, J. Huang, G. Yu, Adsorption of perfluorinated compounds on aminated rice husk prepared by atom transfer radical polymerization, Chemosphere, 91 (2013) 124–130.
[44] W. Zhang, C. Li, M. Liang, Y. Geng, C. Lu, Preparation of carboxylate-functionalized cellulose via solvent-free mechanochemistry and its characterization as a biosorbent for removal of $Pb^{2+}$ from aqueous solution, J. Hazard. Mater., 181 (2010) 468–473.
[45] M. Ji, X. Su, Y.X. Zhao, W.F. Qi, Y. Wang, G.Y. Chen, Z.Y. Zhang, Effective adsorption of Cr(VI) on mesoporous Fe-functionalized Akadama clay: Optimization, selectivity, and mechanism, Appl. Surf. Sci., 344 (2015) 128–136.
[46] D. Park, S.R. Lim, Y.S. Yun, J.M. Park, Development of a new Cr(VI)-biosorbent from agricultural biowaste, Bioresour. Technol., 99 (2008) 8810–8818.
[47] V.M. Boddu, K. Abburi, J.L. Talbott, E.D. Smith, Removal of hexavalent chromium from wastewater using a new composite chitosan biosorbent, Environ. Sci. Technol., 37 (2003) 4449–4456.
[48] S. Chen, Q. Yue, B. Gao, X. Xu, Equilibrium and kinetic adsorption study of the adsorptive removal of Cr(VI) using modified wheat residue, J. Colloid Interface Sci., 349 (2010) 256–264.
[49] K.K. Singh, S.H. Hasan, M. Talat, V.K. Singh, S.K. Gangwar, Removal of Cr (VI) from aqueous solutions using wheat bran, Chem. Eng. J., 151 (2009) 113–121.
[50] Q. Zhong, Q. Yue, B. Gao, Q. Li, X. Xu, A novel amphoteric adsorbent derived from biomass materials: Synthesis and adsorption for Cu(II)/Cr(VI) in single and binary systems, Chem. Eng. J., 229 (2013) 90–98.
[51] S.S. Baral, S.N. Das, G.R. Chaudhury, Y.V. Swamy, P. Rath, Adsorption of Cr(VI) using thermally activated weed Salvinia cucullata, Chem. Eng. J., 139 (2008) 245–255.
[52] M. Shang, Y. Liu, S. Liu, G. Zeng, X. Tan, L. Jiang, X. Huang, Y. Ding, Y. Guo, S. Wang, A novel graphene oxide coated biochar composite: synthesis, characterization and application for Cr(vi) removal, RSC Adv., 6 (2016) 85202–85212.
[53] Z. Hubicki, A. Jakowicz, Studies on sorption of copper(II) complexes with IDA and NTA acids on strongly and weakly basic anion exchangers, Desalination, 155 (2003) 121–130.
[54] A. Wołowicz, Z. Hubicki, Comparison of strongly basic anion exchange resins applicability for the removal of palladium(II) ions from acidic solutions, Chem. Eng. J., 171 (2011) 206–215.
[55] N. Daneshvar, D. Salari, S. Aber, Chromium adsorption and Cr(VI) reduction to trivalent chromium in aqueous solutions by soya cake, J. Hazard. Mater., 94 (2002) 49–61.
[56] M. Bhaumik, H.J. Choi, M.P. Seopela, R.I. McCrindle, A. Maity, Highly effective removal of toxic Cr(VI) from wastewater using sulfuric acid-modified avocado seed, Ind. Eng. Chem. Res., 53 (2014) 1214–1224.